

Change Detection Meets Visual Question Answering

Zhenghang Yuan, *Student Member, IEEE*, Lichao Mou, Zhitong Xiong, *Member, IEEE*, and
Xiao Xiang Zhu, *Fellow, IEEE*

Abstract—The Earth’s surface is continually changing, and identifying changes plays an important role in urban planning and sustainability. Although change detection techniques have been successfully developed for many years, these techniques are still limited to experts and facilitators in related fields. In order to provide every user with flexible access to change information and help them better understand land-cover changes, we introduce a novel task: change detection-based visual question answering (CDVQA) on multi-temporal aerial images. In particular, multi-temporal images can be queried to obtain high level change-based information according to content changes between two input images. We first build a CDVQA dataset including multi-temporal image-question-answer triplets using an automatic question-answer generation method. Then, a baseline CDVQA framework is devised in this work, and it contains four parts: multi-temporal feature encoding, multi-temporal fusion, multi-modal fusion, and answer prediction. In addition, we also introduce a change enhancing module to multi-temporal feature encoding, aiming at incorporating more change-related information. Finally, effects of different backbones and multi-temporal fusion strategies are studied on the performance of CDVQA task. The experimental results provide useful insights for developing better CDVQA models, which are important for future research on this task. The dataset will be available at <https://github.com/YZHJessica/CDVQA>.

Index Terms—Multi-temporal aerial images, visual question answering (VQA), change detection, deep learning

I. INTRODUCTION

THE Earth’s surface is continually changing by man-made and natural influences. These changes are closely involved in human and social development and also guide the urban planning and sustainability [1]. Change detection, aiming at detecting differences of the same region at different times, has become a research priority in recent decades [2]–[4]. Timely and effective change information can be used for many practical applications such as environmental management [5]–[7], natural disasters monitoring [8], [9], urban land-use [10], [11] and agriculture production [12].

This work is jointly supported by the China Scholarship Council, by the European Research Council (ERC) under the European Union’s Horizon 2020 research and innovation programme (grant agreement No. [ERC-2016-StG-714087], Acronym: *So2Sat*), by the Helmholtz Association through Helmholtz Excellent Professorship “Data Science in Earth Observation - Big Data Fusion for Urban Research” (grant number: W2-W3-100), by the German Federal Ministry of Education and Research (BMBF) in the framework of the international future AI lab “AI4EO – Artificial Intelligence for Earth Observation: Reasoning, Uncertainties, Ethics and Beyond” (grant number: 01DD20001) and by the German Federal Ministry for Economic Affairs and Climate Action in the framework of the “national center of excellence ML4Earth” (grant number: 50EE2201C).

Z. Yuan, L. Mou, Z. Xiong and X. X. Zhu are with the Data Science in Earth Observation, Technical University of Munich (TUM), 80333 Munich, Germany. (e-mails: zhenghang.yuan@tum.de; lichao.mou@tum.de; zhitong.xiong@tum.de; xiaoxiang.zhu@tum.de)



Fig. 1. Examples of questions for natural imagery, aerial imagery, and multi-temporal aerial images in VQA tasks.

Nowadays, change detection technology has been developed significantly, and there are various algorithms with great performance improvement for remote sensing data [13]–[15]. Change detection methods can be divided into two main categories, depending on whether or not the types of changes are detected. One is binary change detection that only detects changed regions but ignores the type of changes, e.g., the object-oriented key point vector distance for detecting binary land-cover changes [16] and the end-to-end 2D CNN for hyperspectral image change detection [17]. Change maps obtained by such methods are visualized by binary values to depict change information at the pixel level. The other is semantic change detection, for instance, using asymmetric Siamese network for identifying changes via feature pairs [18] and reasoning bi-temporal semantic correlations [19]. These methods not only detect changed regions but also identify change types.

Although change detection has great application value, the specialized nature of this task makes change information limited to researchers. It is still difficult for end users to access and understand much of important change information. For instance, ordinary users are interested in a certain change type in a certain region, but it is inconvenient and ineffective for them to find it on change maps in practical applications. Considering this problem, efficient and effective change information interaction with end users becomes important. In this context, nature language processing (NLP) enables computers to understand the text in almost the same way as humans. It is user-friendly and can greatly improve the interactivity between image analysis systems and end users. Therefore, in order to alleviate the interaction issue, the integration of computer

vision and NLP [20] has gradually become a hot research topic in the machine learning community. In particular, tasks like visual description generation [21], visual storytelling [22], visual question answering (VQA) [23], [24] and visual dialog [25] have been fully and successfully conducted in computer vision. Similarly, tasks of integrating remote sensing imagery and NLP, such as image captioning and VQA, have also become an active research topic in the field of remote sensing [26], [27]. Captioning for remote sensing images was first proposed in [28], and Lu et al. [29] further explored captioning methods using both handcrafted and convolutional features and proposed a new dataset. Recently, a multilayer aggregated Transformer was utilized to extract information for caption generation [30]. Regarding VQA for remote sensing data (RSVQA), Lobry et al. [31] first introduced this task, built two datasets, and used a hybrid CNN-RNN model to extract feature, and Yuan et al. [32] proposed a self-paced curriculum learning based model trained from easy to hard questions gradually.

Compared to natural images, aerial images are more specialized due to the top-view perspective and complicated background. As shown in Fig. 1, answers to questions about natural images [23] are more obvious than answers to questions about aerial images [31] in many cases in VQA tasks. Besides, Fig. 1 illustrates that answers to questions about the comparison of multi-temporal aerial images require careful observation and even calculation, which is unfriendly to ordinary users. Though VQA for natural images has been studied for many years and VQA for remote sensing data has also gradually become a research focus, VQA for change detection based on multi-temporal images is under-explored. Considering the significance of change detection task and its values in practical applications, it is vital to investigate how to improve the friendliness and accessibility of change detection systems to end users. Hence, there is also a greater need to develop end user accessible VQA algorithms for multi-temporal remotely sensed data.

In this paper, we introduce the task of change detection-based visual question answering (CDVQA) on multi-temporal aerial images. Specifically, given two aerial images captured at different times and a natural language question about them, the CDVQA task aims to provide an answer in natural language by comparing the content of two images. To this end, we create a CDVQA dataset by an automatic generation method, which contains 2,968 pairs of multi-temporal images and more than 122,000 question-answer pairs. The questions are carefully designed to cover various types of changes. Moreover, we propose a baseline method for CDVQA task as shown in Fig. 2. To sum up, the main contributions of this work are summarized as follows:

- We design an automatic question-answer generation method and create a new CDVQA dataset. Specifically, the proposed dataset contains 2,968 pairs of aerial images and more than 122,000 corresponding question-answer pairs.
- A baseline framework for CDVQA task is proposed, and it includes four parts: multi-temporal feature encoding, multi-temporal fusion, multi-modal fusion and answer

prediction. In addition, a change enhancing module is proposed to incorporate more change-related information into visual features.

- Extensive experiments have been conducted to study effects of different network parts on the CDVQA performance. Particularly, different backbones and multi-temporal fusion strategies are investigated. The results provide useful insights on the CDVQA task.

The rest of the paper is organized as follows. The detailed information for the construction of CDVQA dataset is introduced in Section II. Section III presents the methodology. Experimental results and discussion are shown in Section IV. Finally, this paper is concluded in Section V.

II. DATASET

Different from the traditional VQA task, CDVQA involves multi-temporal aerial images and requires time series analysis. Taking this into account, we choose the existing semantic change detection dataset SECOND [18] as the basic data to automatically generate a CDVQA dataset. The SECOND dataset collects bi-temporal high resolution optical (RGB) images by several different aerial platforms and sensors, with spatial resolution varying from 0.5 m to 3 m [19]. Geographical positions include several cities in China, such as Shanghai, Hangzhou, and Chengdu. It has 4,662 pairs of aerial images with the size of 512×512 pixels, and 2,968 pairs are publicly available. Each pair consists of a pre-event aerial image and a post-event image of the same location at different times. Besides, each pair has two labeled semantic change maps at the pixel level, before and after the change. In each semantic change map, non-change region and 6 land-cover classes related to changes including non-vegetated ground (NVG) surface, buildings, playgrounds, water, low vegetation and trees are annotated. The authors of the SECOND dataset declare in their paper that semantic change maps in this dataset are labeled by a team of experts in Earth vision applications and high accuracy is guaranteed. Therefore, the generated question-answer pairs in this work are highly relevant to the content of image pairs. Overall, this dataset has critical semantic change information of main land-cover classes at pixel-level, which provides sufficient information for generating question-answer pairs for the CDVQA task. In this case, we use the 2,968 openly available pairs as our basic data for the further dataset construction.

A. Multi-temporal Image-Question-Answer Triplets Construction

Formally, in each pair of multi-temporal aerial images, let $\mathbf{x}_{t_1} \in \mathbb{R}^{3 \times H \times W}$ be the image at time T_1 , and $\mathbf{x}_{t_2} \in \mathbb{R}^{3 \times H \times W}$ be the image at time T_2 . $\mathbf{s}_{t_1} \in \mathbb{R}^{H \times W}$ and $\mathbf{s}_{t_2} \in \mathbb{R}^{H \times W}$ denote semantic change maps of \mathbf{x}_{t_1} and \mathbf{x}_{t_2} , respectively, and each pixel in \mathbf{s}_{t_1} and \mathbf{s}_{t_2} indicates one semantic class, ranging from 0 to 6. Semantic change maps show changed regions and provide their change types at the pixel level. Background pixels mean non-change regions, which are the same in both \mathbf{s}_{t_1} and \mathbf{s}_{t_2} for an image pair. Foreground pixels indicate changed regions of different land-cover types. Specifically, the

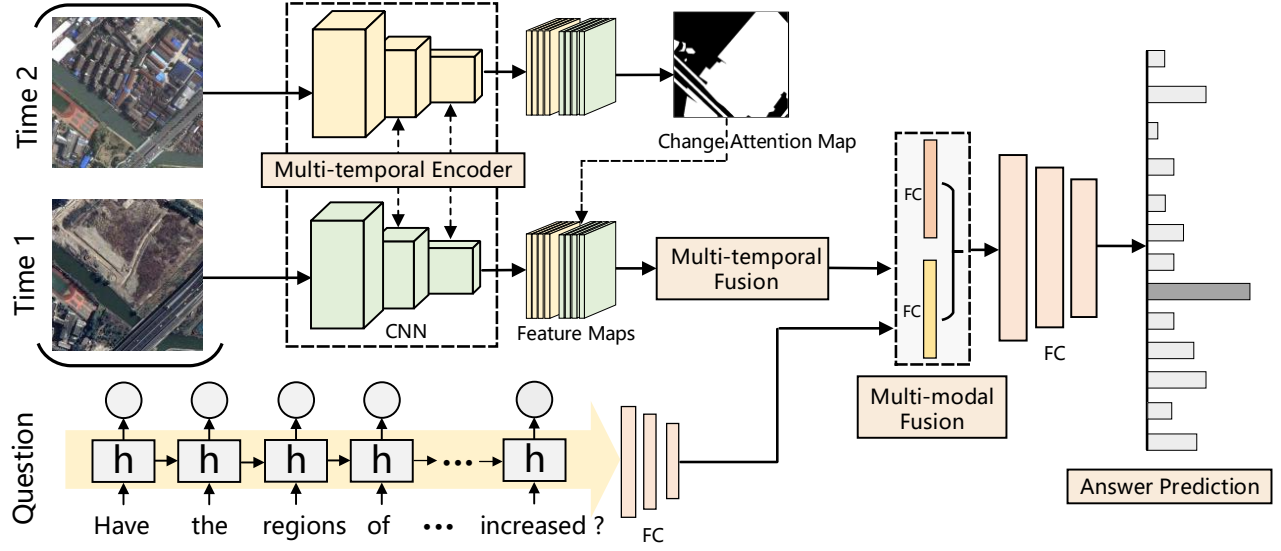


Fig. 2. The main architecture of the proposed CDVQA framework. It contains four main parts: multi-temporal feature encoding, multi-temporal fusion, multi-modal fusion, and answer prediction.

value of the pixel in s_{t_1} indicates the semantic class at T_1 and the value of the pixel in s_{t_2} indicates the semantic class at T_2 . The main advantage of introducing semantic change maps is that we can access more details about changes, i.e., we are able to know not only where changes happen but also what types they are. In this work, our motivation is to use natural language as queries to obtain these two types of information. Given semantic change information of s_{t_1} , s_{t_2} , the following five types of questions are designed in the proposed dataset: *change or not*, *increase/decrease or not*, *change to what*, *largest/smallest change*, and *change ratio*. In our case, the smallest/largest change refers to the land cover class that has the least/most pixels changing. These questions are of great interest to end users in real-world applications. In what follows, a detailed description of the automatic generation of multi-temporal image-question-answer triplets for different question types is given.

- **Change or not.**

Change or not for an image pair. The most fundamental yet important information in change detection is about whether a certain land-cover has changed. Note that a change occurs regardless of whether the area of a land-cover increases or decreases. For each pair of aerial images, the set of changed land-cover classes \mathcal{L}_{t_1} and \mathcal{L}_{t_2} are extracted from s_{t_1} and s_{t_2} , respectively. Let l_i be a land-cover class, $l_i \in \mathcal{L}_{t_1}$ or $l_i \in \mathcal{L}_{t_2}$, indicating that the corresponding land-cover type has changed. In this case, the answer should be *yes*. On the contrary, if $l_i \notin \mathcal{L}_{t_1}$ and $l_i \notin \mathcal{L}_{t_2}$, it indicates that the corresponding land-cover does not change. Then, the answer should be *no*. All land-cover types are traversed to generate multiple question-answer pairs.

Change or not for a single image. For change detection tasks, sometimes one want to focus not only on whether a certain land-cover class has changed, but also on whether

changes have occurred in the pre-event image or post-event image. Therefore, we extract semantic change information solely from the first or second image to generate relevant questions and answers. Please note that in this work, the first image in the image pair refers to the pre-event/pre-change, and the second image means the post-event/post-change. Particularly, for the land-cover class l_i , if $l_i \in \mathcal{L}_{t_1}$, it indicates that the corresponding land-cover has changed on the pre-event image. The answer under this situation should be *yes*. Similarly, if $l_i \in \mathcal{L}_{t_2}$, it means that the area of l_i has changed on the post-event image. The answer will also be *yes*. In other cases, i.e. $l_i \notin \mathcal{L}_{t_1}$ and $l_i \notin \mathcal{L}_{t_2}$, the corresponding answer to the question about whether it has changed on a single image should be *no*.

- **Increase/decrease or not.**

Change detection in real-world applications often requires more specific change information, for instance, whether the area of a land-cover has increased or decreased. In this context, we denote the area of l_i in s_{t_1} as $A_{t_1}^i$ and the area in s_{t_2} as $A_{t_2}^i$. For increasing-related question-answer pairs, if $A_{t_2}^i - A_{t_1}^i > 0$, the area of l_i increases. Then the answer to this question should be *yes*. For decreasing-related pairs, the generation process is similar. If $A_{t_2}^i - A_{t_1}^i < 0$, the area of l_i decreases. Note that the area of l_i is defined as all pixels with label l_i in the whole imagery.

- **Change to what.**

This type of questions involves more detailed information about changes, i.e., what the land-cover at time T_1 mainly becomes to at time T_2 . Such questions require analyzing the same region in multi-temporal images to obtain the change of land-cover types in this region. Although one class may change to more than one class over time, it is more meaningful to focus on the major change.

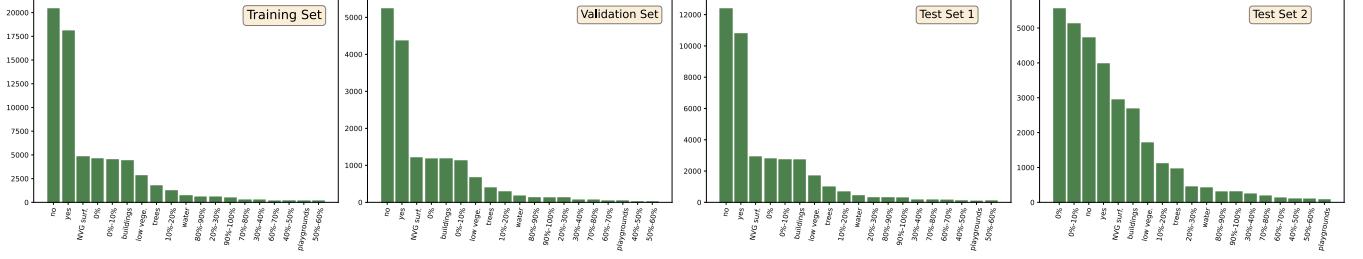


Fig. 3. Visualization of answer distributions of different subsets. From left to right: training set, validation set, test set 1, and test set 2.

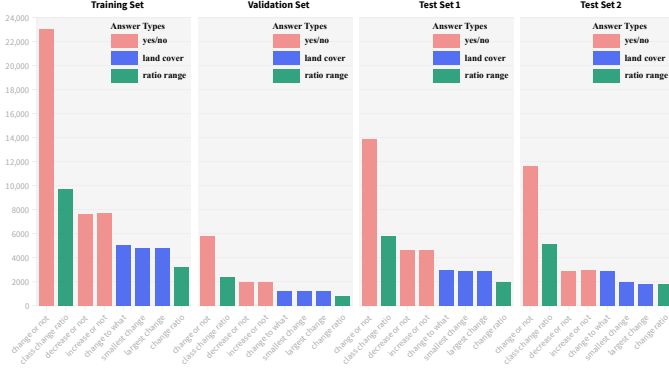


Fig. 4. Visualization of question distributions of different subsets. From left to right: training set, validation set, test set 1, and test set 2.

Particularly, for a semantic class, we first find its pixel indices in s_{t_1} . Then, the indices are used to select the corresponding pixels in s_{t_2} . Finally, we count the number of the selected pixels for each land-cover type and choose the type with the largest number as the major change. In this case, the answer to the question what the regions of l_i at time T_1 mainly change to should be the major change type.

- **Largest/smallest change.**

Largest/smallest change for an image pair. Such questions focus on the largest or smallest changes in multi-temporal images. For each land-cover type, all changes in the two images should be taken into account. Therefore, the changed area for the land-cover class l_i is $A_{t_1}^i + A_{t_2}^i$. By traversing all change types, the maximum and minimum changed regions can be obtained, and the corresponding land-cover classes are answers to this type of questions. In this dataset, the smallest change is which has the smallest changed area, and the unchanged type is not considered.

Largest/smallest change for a single image. To extract more detailed information about changes, we also analyze the maximum and minimum changed regions for the pre-event and post-event image separately. The maximum and minimum changed regions at time T_1 can be easily obtained by $\arg \max_{l_i}(A_{t_1}^i)$ and $\arg \min_{l_i}(A_{t_1}^i)$, and the

selected land-cover l_i is the corresponding answer. For time T_2 , the generation process is the same. This type of questions requires a model to not only identify land-cover changes in bi-temporal images but also understand which image (T_1 or T_2) is queried by users. In this context, the question “What is the smallest change in the first image?” is actually asking about the land-cover of the smallest changed region in the image captured at an earlier date.

- **Change ratio.**

Change ratio for all land-covers. The percentages of changed regions are also very important information in practical applications. The change ratio can be calculated via dividing the changed area by the total area of the whole map, and the same for non-change ratio. Since proportions are continuous numbers, they cannot be compatible with the classification task. Thus, we discretize ratios into bins. To be more specific, numerical answers are quantized into 11 categories: 0%, 0%-10%, 10%-20%, 20%-30%, 30%-40%, 40%-50%, 50%-60%, 60%-70%, 70%-80%, 80%-90%, and 90%-100%. Notice that in this context $A\%-B\%$ means $(A, B]$. In this way, we calculate the change percentage for each image pair and gain answers to the change ratio-related questions.

Change ratio for each land-cover. In addition to the ratio of all changed regions, we also want to analyze the change ratio for each land-cover class on the pre-event or post-event image. Similarly, numerical answers are also quantized as above. For each land-cover class l_i , we first calculate its changed regions $A_{t_1}^i$ and $A_{t_2}^i$ at T_1 and T_2 . Then, the change ratio for l_i on the pre-event image is calculated via dividing $A_{t_1}^i$ by the total area of the whole image. In the same way, change ratios for different land-covers on the post-event image can be obtained.

In practice, we have defined multiple synonymous templates for each type of questions. During the question-answer generation process, for each image pair, question-answer pairs are generated separately for each question type. As more than one template is designed for each question type, we randomly select one of them to generate a sample. To balance the number of samples in each question type, we set different probabilities for generating samples of different question types. Specifically, we set a low probability value for the “yes/no” type and a high probability value for other question types. For each image pair, we generate 16 samples in average.

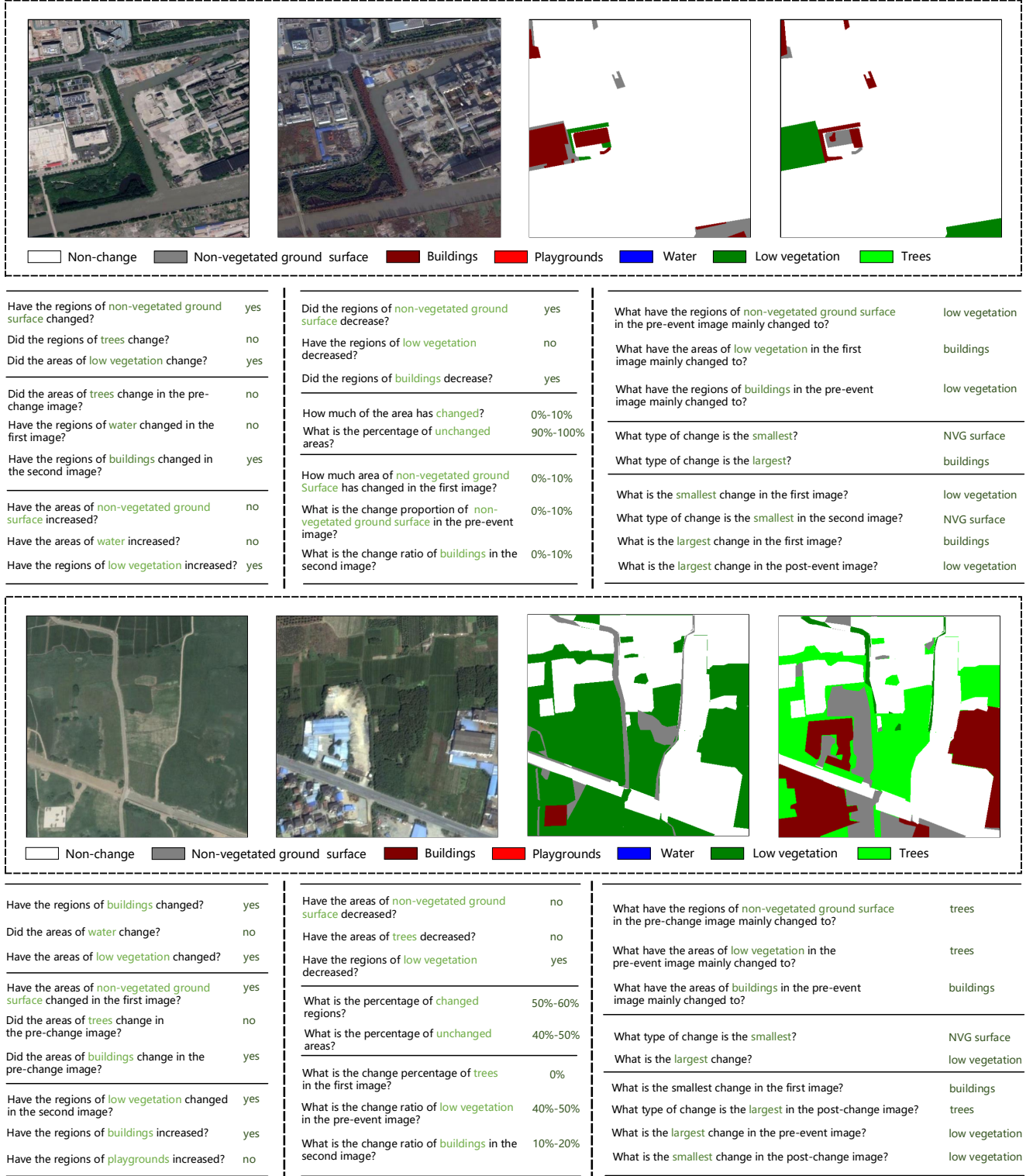


Fig. 5. Visualization examples of the generated CDVQA dataset. Here, we show two data samples, and each one contains bi-temporal images, questions, and the corresponding answers. Best viewed in color and zoomed in.

B. Question and Answer Distributions

As 2,968 pairs of images are publicly available, we use these images as the basic data to generate the CDVQA dataset. The whole dataset is split into the training set, validation set, and test set. To better evaluate the robustness and reliability of CDVQA models, we generate two test sets with different distributions of answers. The class distributions of answers in the generated CDVQA dataset are displayed in Fig. 3. From this figure, we can see that the training set, validation set, and test set 1 share the same class distribution. The answer distributions of test set 1 and test set 2 are different.

As we can see from Fig. 3, answer types in all subsets obey the long-tail distribution. Concretely, answer class *no* dominates answer distributions in all subsets. For example, in the training set, samples with answer *no* occupy 30.9% of all instances. In the test set 1, answers *no* account for 31.15% of total answers. In contrast, answers *50%-60%* only occupy 0.22% of all answers. The reason for the class imbalance is that there are more questions asking for *yes* or *no*. The answers to questions such as *change or not* and *increase/decrease or not* are *yes* or *no*.

The question type distributions of all four subsets are presented in Fig. 4. For simplicity, *change ratio for each land-cover* is denoted as *class change ratio*. We can see that distributions of question types are also long-tailed. In addition, question type *change or not* has the highest frequencies in all subsets. This is the reason why the two most frequent answer types are *yes* and *no*. Similar to answer distributions, the distributions of question types for the training set, validation set, and test set 1 are the same, while they are different from the distribution of the test set 2. Specifically, the proportions of questions about “change to what”, “change ratio”, and “class change ratio” increase in test set 2 compared to test set 1. Since questions of these types are more difficult, test set 2 is more difficult than test set 1. Visualization examples of the generated CDVQA dataset are shown Fig. 5.

III. METHODOLOGY

In this work, the CDVQA task is deemed as a classification task. Note that semantic change maps are only used to generate question-answer pairs in the dataset preparation phase, and in CDVQA, only image pairs, questions, and the corresponding answers are used for training and evaluating a model. As shown in Fig. 2, our CDVQA model takes as input two aerial images and a question. The output of the model is an answer predicted by the network. Particularly, the whole network architecture consists of four parts. The first component is a multi-temporal visual feature learning module which is used to encode the input images into deep features. The second part, named multi-temporal fusion, is responsible for fusing the features of the two images. The third one is a multi-modal fusion module that aims at fusing the image and question features. The forth is an answer prediction part, which takes the fused multi-modal feature as input to predict the answer. In addition, for CDVQA task, we design a change enhancing module to encourage the model to focus on changed pixels of the input images. The proposed modules in our

CDVQA framework will be described in detail in the following subsections.

A. Multi-temporal Encoder

Different from tasks like image classification, object detection, and semantic segmentation, change analysis involves two input images of the same location but at different times. Similarly, a CDVQA system takes as input multi-temporal inputs. In order to identify changes between two images, temporal differences should be extracted and analyzed.

In respect of multiple inputs, Siamese networks are commonly used in many vision tasks. We denote the feature of the image of time T_1 as $F_1 = f_1(x_{t_1})$. Likewise, $f_2(\cdot)$ is used to obtain the encoded representation for the image of time T_2 . For Siamese networks, we set the network architecture and parameters of f_1 and f_2 to be the same.

In this work, we explore effects of different encoder networks on CDVQA. For visual feature extraction, convolutional neural networks (CNNs) are usually used to learn feature representations, and ResNet [33] is an important milestone in the development of CNN architectures. Thus, different scales of ResNets, e.g., ResNet-18, ResNet-101, and ResNet-152, are employed as the multi-temporal encoder of our CDVQA model, aiming at studying effects of different scales of CNNs on CDVQA.

Recently, Transformer architecture [34] has achieved excellent performance on NLP tasks [35]. Designed for sequence modeling tasks, Transformer has the significant advantage of using attention to learn long-range dependencies in data. Considering its great success in the language modeling domain, it has also been applied to computer vision tasks, to name a few, image classification [36], [37], object detection [38], and semantic segmentation [39]. In this work, the Transformer-based encoder for multi-temporal images is also used.

B. Change Enhancing Module

Change detection is a fundamental task in remote sensing and also the core of CDVQA task. To answer change-related questions, a model needs to focus on changed regions and further analyze semantic information. In a number of computer vision tasks, self-attention mechanism [40]–[42] is used to boost the performance by focusing on important parts of data samples. However, there are two input images in our case, where the self-attention mechanism is not applicable. Hence, in this work, we propose a change enhancing module to enhance the CDVQA model in terms of the capability of detecting changes.

We denote that the encoded deep features for the input two images are $F_1 \in \mathbb{R}^{N \times C \times H \times W}$ and $F_2 \in \mathbb{R}^{N \times C \times H \times W}$, respectively, where N is batch size, C is the number of channels, and H, W are the height and width of feature maps. The conventional self-attention model [34] first transforms the input feature into three independent features, i.e., the query Q , key K , and value V . In contrast, for the proposed change enhancing module, we treat the feature representations F_1

and F_2 as the query and key, respectively, and compute their similarity $F_s \in \mathbb{R}^{N \times C \times H \times W}$ as follows:

$$F_s = |f_q(F_1) - f_k(F_2)|, \quad (1)$$

where $f_q(\cdot)$ and $f_k(\cdot)$ are 1×1 convolutions for the purpose of feature transformation. Next, a change enhancing map $M_{ce} \in \mathbb{R}^{N \times H \times W}$ can be obtained by:

$$M_{ce} = \sigma(f_c(F_s)), \quad (2)$$

where $f_c(\cdot)$ is a 1×1 convolution layer for predicting the change enhancing map. $\sigma(\cdot)$ is ReLU activation function. The map M_{ce} is used to encourage the model to focus on regions where differences between F_1 and F_2 are large. To this end, we scale M_{ce} with a parameter θ and add it with an identity matrix I . θ is a learnable parameter with an initial value of 0 and is optimized during training in an end-to-end manner. Then, we multiply the transformed M_{ce} and two encoded features, respectively:

$$\begin{aligned} F_{c1} &= (I + \theta M_{ce})F_1, \\ F_{c2} &= (I + \theta M_{ce})F_2, \end{aligned} \quad (3)$$

where F_{c1} and F_{c2} are the final encoded features corresponding to two input images. F_{c1} and F_{c2} will then be fused by the multi-temporal feature fusion module, which will be introduced in the next subsection.

C. Multi-temporal Fusion

After the feature encoding and change enhancing processing, we need to fuse features of time T_1 and time T_2 to obtain the final visual feature F_v . For the fusion of multiple feature maps, element-wise subtraction, multiplication, summation, and concatenation are commonly used methods. Given two feature maps $F_{c1} \in \mathbb{R}^{N \times C \times H \times W}$ and $F_{c2} \in \mathbb{R}^{N \times C \times H \times W}$, the aforementioned fusion methods can be formulated as:

$$\begin{aligned} F_{v1} &= F_{c1} \ominus F_{c2}, \\ F_{v2} &= \frac{F_{c1}}{\|F_{c1}\|_2} \ominus \frac{F_{c2}}{\|F_{c2}\|_2}, \\ F_{v3} &= F_{c1} \frown F_{c2}, \\ F_{v4} &= F_{c1} \oplus F_{c2}, \\ F_{v5} &= F_{c1} \otimes F_{c2}, \end{aligned} \quad (4)$$

where \ominus denotes element-wise subtraction operation. Note that we normalize the two features before the element-wise subtraction operation for computing F_{v2} . \oplus and \otimes denote element-wise summation and multiplication operations, respectively. \frown stands for the concatenation operation along the channel dimension. To study effects of different fusion strategies, we compare and analyze their performance in Section IV.

D. Multi-modal Fusion

Since CDVQA involves both visual features and language representations, we need to fuse multi-modal features. After the multi-temporal feature fusion, the final visual representation $F_v \in \mathbb{R}^{N \times C \times H \times W}$ can be obtained. Meanwhile, a recurrent neural network (RNN) is used to encode the question

TABLE I
NUMERICAL RESULTS OF USING DIFFERENT BACKBONE NETWORKS ON THE TEST SET 1 OF CDVQA DATASET.

Question Types	ResNet-18	ResNet-101	ResNet-152	ViT-B16
change ratio	0.3455	0.3388	0.3476	0.3600
class change ratio	0.7200	0.7134	0.7115	0.7231
change or not	0.8379	0.8387	0.8374	0.8401
change to what	0.5710	0.5737	0.5770	0.5820
increase or not	0.6913	0.6902	0.6854	0.6952
decrease or not	0.7303	0.7243	0.7275	0.7185
smallest change	0.2627	0.2758	0.2734	0.2710
largest change	0.4603	0.4576	0.4669	0.4648
Average Accuracy	0.5773	0.5766	0.5783	0.5818
Overall Accuracy	0.6771	0.6763	0.6766	0.6800

into feature vector $V_q \in \mathbb{R}^{N \times L}$. As the skip-thoughts model has been applied in many remote sensing image-based NLP tasks [31], [43], we choose to use the pre-trained skip-thoughts model [44] for the language feature extraction part. Specifically, skip-thought vectors are modeled with an encoder-decoder architecture, and both are constructed with RNNs. The encoder transforms the input sentence into a vector, and two decoders are used to decode the vector into the previous and the next sentence, respectively. In this work, we use the encoder of skip-thoughts for generating language embeddings.

Before fusing features of two modalities, we first transform the visual feature F_v into a feature vector $F_{vt} \in \mathbb{R}^{N \times L}$. Then, the two feature vectors have the same size, and we can fuse F_{vt} and V_q together. As how to fuse them is not the main research content of this work, we simply merge them into a multi-modal feature by concatenation:

$$F_m = V_q \frown F_{vt}, \quad (5)$$

where $F_m \in \mathbb{R}^{N \times 2L}$ is the fused multi-modal representation.

Finally, as the answer prediction is modeled as a classification task in this work. The feature F_m is used to predict the answer by passing through a classifier, i.e., two fully connected layers. The answer is given by selecting the answer class with the highest probability. The output dimension of the first layer is 256 and the final output dimension of the classifier is 19, as there are 19 answer types. Specifically, the possible answers include no, yes, 0%-10%, 0, NVG surface, buildings, low vegetation, 10%-20%, trees, 20%-30%, water, 80%-90%, 30%-40%, 90%-100%, 70%-80%, 40%-50%, 60%-70%, 50%-60%, and playgrounds (sorted by the number of samples).

IV. EXPERIMENTS

A. Datasets

The CDVQA dataset is publicly available in 2,968 image pairs with the size of 512×512 . Based on these image pairs, there are more than 122,000 question-answer pairs generated in total. The training, validation, and test sets are split based on image pairs captured at different geographical positions. Particularly, the training set contains 65,967 question-answer pairs, which are generated from 1,600 (53.91%) image pairs. There are 16,441 question-answer pairs in the validation set, which are produced based on 400 (13.48%) image pairs.

TABLE II
NUMERICAL RESULTS OF USING DIFFERENT BACKBONE NETWORKS ON
THE TEST SET 2 OF CDVQA DATASET.

Question Types	ResNet-18	ResNet-101	ResNet-152	ViT-B16
change ratio	0.3444	0.3465	0.3588	0.3651
class change ratio	0.7131	0.7158	0.7142	0.7174
change or not	0.7818	0.8363	0.8403	0.8353
change to what	0.5316	0.5693	0.5705	0.5790
increase or not	0.7003	0.6880	0.7012	0.6847
decrease or not	0.7142	0.7331	0.7264	0.7303
smallest change	0.2000	0.2803	0.2568	0.2592
largest change	0.3793	0.4607	0.4637	0.4665
Average Accuracy	0.5456	0.5787	0.5790	0.5797
Overall Accuracy	0.6165	0.6333	0.6336	0.6341

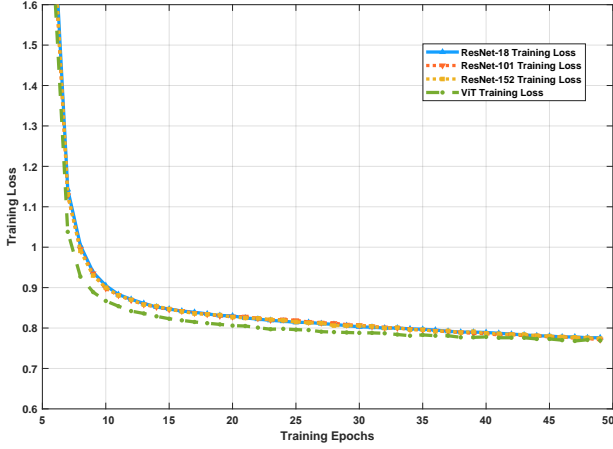


Fig. 6. Visualization of training losses. Four different backbone networks are compared.

Besides, we use the left 968 (32.61%) image pairs to generate two test sets with 39,686 (test set 1) and 31,036 (test set 2) question-answer pairs for more comprehensive model evaluation. Note that there is an overlap between the two test sets.

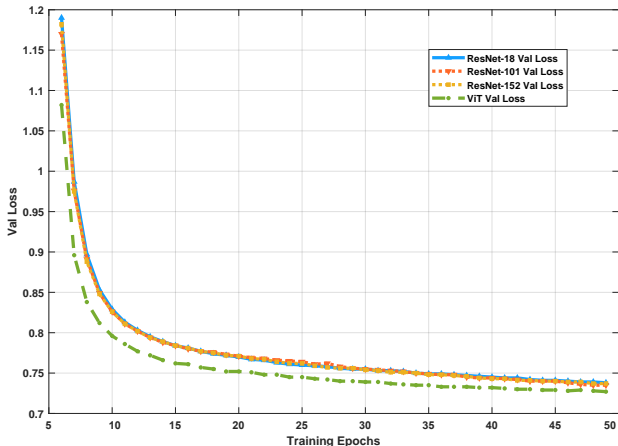


Fig. 7. Visualization of validation losses. Four different backbone networks are compared.

B. Implementation Details

The generated dataset for CDVQA follows the same format as the work of RSVQA [31]. Regarding training parameters, Adam optimizer is used with an initial learning rate of $1e-4$. For all ResNet-based models, the batch size is set to 70, and the size of the input image is scaled to 256×256 . Since the used ViT [37] model requires the input size to be 384×384 , we have to reduce the batch size to 32 considering GPU memory limit. For all experiments, 50 epochs are used to train models. We utilize accuracy as a measurement for each question type. Additionally, average accuracy and overall accuracy are also reported.

C. Effects of Different Backbones







The backbone network of the visual encoder is an important component. Therefore, we compare four different backbones: three ResNets (ResNet-18, ResNet-101, and ResNet-152) and a vision Transformer model ViT. In all experiments, we fuse multi-temporal visual features by feature concatenation for all backbone networks.







The results on two different test sets are displayed in Table I and Table II, respectively. From the results, we can see that compared to ResNet-18 and ResNet-101, ResNet-152 does not show a significant performance advantage. For example, on the test set 1, ResNet-18 and ResNet-152 deliver very close average and overall accuracies. This indicates that merely improving the capability of backbone network for visual learning only yields a limited gain. However, when we change the network architecture of the backbone from ResNet to Transformer, the performance can be further improved. The reason for this improvement is that the self-attention mechanism of Transformer networks is beneficial for learning more representative features. Note that parameters of backbone networks are fixed during the training stage. In Fig. 6 and Fig. 7, we also visualize training and validation losses of models with different backbones. It can be seen that the ViT backbone has significantly lower losses than ResNet-based networks. Note that we omit the first 5 epochs to better compare the final convergence state.







From the results, we can see that different backbone networks have very little impact on the performance of our framework. This is because visual feature learning may not be the key to improving accuracy. Other parts of the model, such as multi-temporal fusion and change analysis part, may be more critical for the performance improvement of the CDVQA task.

D. Effects of Different Multi-temporal Fusion Strategies

In this subsection, we quantitatively compare five commonly-used feature fusion operations, namely concatenation (Concat), summation (Sum), subtraction (Sub), normalized subtraction (NSub), and multiplication (Mul). The numerical results on two test sets are presented in Table III and Table IV. The results in these tables show that concatenation is the best. The concatenation operation first concatenates two inputs together, and then several fully-connected layers are

											
What is the change proportion of buildings in the second image?				What is the percentage of changed regions ?				What is the change ratio of trees in the post-event image?			
Label: 0%-10%		Predicted: 0%-10%		Label: 10%-20%		Predicted: 10%-20%		Label: 0%-10%		Predicted: 0%	

											
Did the areas of buildings increase?				What type of change is the smallest in the pre-event image?				What do the regions of non-vegetated ground surface in the first image mainly changed to?			
Label: No		Predicted: No		Label: NVG surface		Predicted: NVG surface		Label: Trees		Predicted: Buildings	

											
Have the areas of low vegetation changed in the second image?				What is the smallest change?				What type of change is the smallest in the pre-event image?			
Label: Yes		Predicted: Yes		Label: Buildings		Predicted: Buildings		Label: Low vegetation		Predicted: NVG surface	







											
Did the areas of trees change in the pre-change image?				Has the areas of non-vegetated ground surface changed in the second image?				Have the regions of buildings decreased?			
Label: No		Predicted: No		Label: Yes		Predicted: Yes		Label: Yes		Predicted: No	

Fig. 8. Visualization examples of CDVQA results. Each row presents three different questions and the same input image pair. Correctly predicted results are shown in blue, and wrong answers are in red.

TABLE III
NUMERICAL RESULTS OF USING DIFFERENT FUSION STRATEGIES ON
THE TEST SET 1 OF CDVQA DATASET.

ResNet-101	Concat \cup	Sub \ominus	NSub \ominus	Mul \otimes	Sum \oplus
change ratio	0.3388	0.3182	0.3151	0.3047	0.3352
class change ratio	0.7134	0.7129	0.7130	0.7131	0.7167
change or not	0.8387	0.8249	0.8245	0.8271	0.8378
change to what	0.5737	0.5269	0.5543	0.5693	0.5690
increase or not	0.6902	0.6897	0.6919	0.6967	0.6891
decrease or not	0.7243	0.6983	0.7056	0.7020	0.7239
smallest change	0.2758	0.2778	0.2789	0.2799	0.2703
largest change	0.4576	0.4473	0.4411	0.4290	0.4476
Average Accuracy	0.5766	0.5620	0.5655	0.5652	0.5737
Overall Accuracy	0.6763	0.6631	0.6657	0.6665	0.6746

TABLE IV
NUMERICAL RESULTS OF USING DIFFERENT BACKBONE NETWORKS ON
THE TEST SET 2 OF CDVQA DATASET.

ResNet-101	Concat \cup	Sub \ominus	NSub \ominus	Mul \otimes	Sum \oplus
change ratio	0.3465	0.3223	0.3243	0.3119	0.3409
class change ratio	0.7158	0.7097	0.7103	0.7104	0.7169
change or not	0.8363	0.8195	0.8228	0.8148	0.8347
change to what	0.5693	0.5275	0.5549	0.5396	0.5690
increase or not	0.6880	0.6986	0.7146	0.7036	0.6886
decrease or not	0.7331	0.7029	0.7046	0.7172	0.7423
smallest change	0.2803	0.2792	0.2796	0.2799	0.2679
largest change	0.4607	0.4442	0.4428	0.4290	0.4486
Average Accuracy	0.5787	0.5630	0.5692	0.5632	0.5761
Overall Accuracy	0.6333	0.6199	0.6244	0.6196	0.6313

used to fuse these inputs by learnable weights. This makes it a more flexible and general fusion strategy.

For change analysis tasks, intuitively, subtraction should be the best fusion method, as it can better highlight changed regions. However, it can be seen from the results that the subtraction operation cannot outperform others. Considering that the direct subtraction of two features may undermine their representability, we normalize two input features by using ℓ_2 normalization before the subtraction operation. Nevertheless, the normalized subtraction operation is still no better than concatenation and summation. This indicates that directly subtracting two inputs is not useful to CDVQA tasks, and a specific change analysis module should be designed.

E. Effect of Change Enhancing Module

It is critical to obtain semantic change information from multi-temporal images. However, there are no pixel-wise ground truth change labels available in this task. To incorporate change information into the model, we propose a change enhancing module to highlight changed regions in the input images. To validate the effectiveness of the module, we conduct an ablation study, and numerical results are displayed in Table V and Table VI. In the two tables, change enhancing module is abbreviated as CEM for the sake of simplification. The experimental results on both test sets indicate that the proposed change enhancing module is beneficial to the CDVQA task. In particular, from the results in two tables, it can be seen

that the proposed module can consistently improve both the average accuracy and overall accuracy.

F. Cross-dataset Evaluation

In order to explore the generalization ability of the model, we construct another CDVQA dataset as an additional test set. Specifically, we collect 138 image pairs of size 256×256 from HTCD [45] dataset (only binary change maps are available) and manually annotate semantic change maps. Then, 3,303 question-answer pairs are generated and used for the cross-dataset test setting. To show the effectiveness of the proposed method, we compare the performance of a model trained on the CDVQA dataset and another model with randomly initialized weights. Table VII shows numerical results. We can see that the model trained on our CDVQA dataset can be transferred to unseen scenarios, but its performance is not satisfactory in this cross-dataset test setting. This is mainly because there is a domain gap between the tests set of CDVQA and this one. We see that much more research efforts are needed in this direction.

G. Discussion

Regarding numerical results, generally, the average accuracy is lower than 60%, and the overall accuracy is lower than 70%. Some visualization examples of CDVQA results are presented in Fig. 8. Both correctly predicted examples and failures are displayed. From the experimental results, we can conclude that CDVQA is a complex and challenging task. To correctly answer different types of questions, a model first needs to learn multi-modal representations for the input images and questions. Visual and language understanding is of great importance for the model. Besides, CDVQA also requires the model to be able to analyze semantic change information. I.e., the model needs to not only locate changed areas, but also identify land-cover classes of changed regions to answer some complex questions. Currently, the proposed baseline framework does not make use of semantic change labels. Thus its performance on questions related to land-cover classes is not that satisfactory. Change ratio for each land-cover has higher accuracy than change ratio for all land-covers. This is mainly because the former has more training samples. We also visualize the normalized confusion matrix in Fig. 9. Note that the confusion matrix is normalized along the predicted label axis.

To better understand what the model has learned for making decisions, we visualize attention maps of our model on some examples in Fig. 10. It can be seen that the model learns to focus on the related changed regions to predict answers. From experimental results, we can conclude that more research efforts are needed to reach a satisfactory performance on the challenging CDVQA task. Specifically, more effective change analysis-based visual learning methods should be investigated. We also see that Transformer-based models have great potential for multi-temporal and multi-modal feature learning in CDVQA tasks. Additionally, self-supervised or unsupervised change detection methods need to be studied. How to obtain the semantic change information from multi-temporal data in

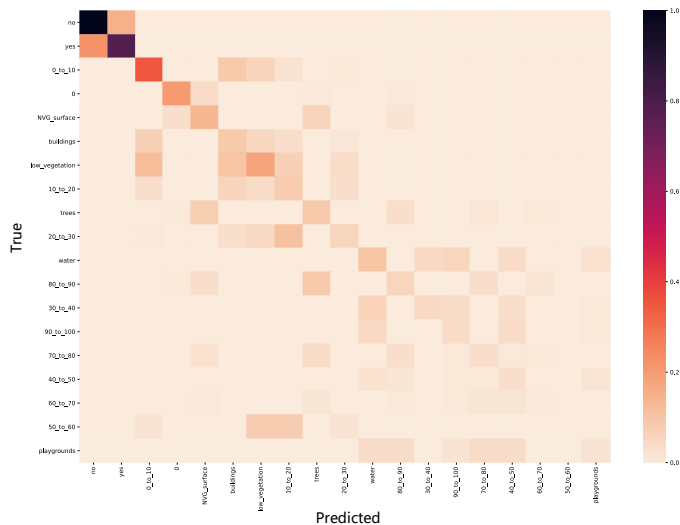


Fig. 9. Normalized confusion matrix for our CDVQA dataset on the test set 1 (ResNet-152 is used as the backbone).

TABLE V
ABLATION STUDY ON THE TEST SET 1 OF CDVQA DATASET FOR
RESNET-101 BACKBONE.

Question Types	w/o CEM	w/ CEM
change ratio	0.3388	0.3854
class change ratio	0.7134	0.7071
change or not	0.8387	0.8292
change to what	0.5737	0.5804
increase or not	0.6902	0.7443
decrease or not	0.7243	0.7697
smallest change	0.2758	0.3127
largest change	0.4576	0.4777
Average Accuracy	0.5766	0.6008
Overall Accuracy	0.6763	0.6903

TABLE VI
ABLATION STUDY ON THE TEST SET 2 OF CDVQA DATASET FOR
RESNET-101 BACKBONE.

Question Types	w/o CEM	w/ CEM
change ratio	0.3465	0.3904
class change ratio	0.7158	0.7714
change or not	0.8363	0.8123
change to what	0.5693	0.6511
increase or not	0.6880	0.7534
decrease or not	0.7331	0.7868
smallest change	0.2803	0.2431
largest change	0.4607	0.3766
Average Accuracy	0.5787	0.5982
Overall Accuracy	0.6333	0.6513

TABLE VII
EXPERIMENTAL RESULTS IN THE CROSS-DATASET TEST SETTING.

Question Types	Random init.	Ours
change ratio	0.0442	0.0615
class change ratio	0.0362	0.0751
change or not	0.0730	0.2042
change to what	0.0722	0.0834
increase or not	0.0382	0.4713
decrease or not	0.0837	0.4659
smallest change	0.0434	0.1413
largest change	0.0724	0.1557
Average Accuracy	0.0601	0.1969
Overall Accuracy	0.0559	0.1560

an unsupervised manner is also an important research direction in CDVQA tasks.

V. CONCLUSION

To provide ordinary end users with flexible access to change information, we introduce a new task named CDVQA with natural language as output. This task takes multi-temporal aerial images and a natural question as inputs to predict the corresponding answer. To be specific, we create a new dataset, which contains 2,968 pairs of aerial images and more than 122,000 question-answer pairs. In addition, a baseline CDVQA model is devised, and different components of models are evaluated on the generated dataset. The experimental results outline possible problems that are needed to be addressed for the CDVQA task. This work also provides some useful insights for developing better CDVQA models, which are important for future research in this direction.

ACKNOWLEDGMENT

We acknowledge the SECOND dataset contributors from Wuhan University and Ca’ Foscari University of Venice.

REFERENCES

- [1] Sudipan Saha, Francesca Bovolo, and Lorenzo Bruzzone, “Building change detection in VHR SAR images via unsupervised deep transcod-ing,” *IEEE Transactions on Geoscience and Remote Sensing*, vol. 59, no. 3, pp. 1917–1929, 2020.
- [2] Yifang Ban and Osama Yousif, “Change detection techniques: A review,” *Multitemporal Remote Sensing*, pp. 19–43, 2016.
- [3] Yanan You, Jingyi Cao, and Wenli Zhou, “A survey of change detection methods based on remote sensing images for multi-source and multi-objective scenarios,” *Remote Sensing*, vol. 12, no. 15, pp. 2460, 2020.
- [4] Marrit Leenstra, Diego Marcos, Francesca Bovolo, and Devis Tuia, “Self-supervised pre-training enhances change detection in Sentinel-2 imagery,” *arXiv preprint arXiv:2101.08122*, 2021.
- [5] Jiaojiao Tian, Allan Aasbjerg Nielsen, and Peter Reinartz, “Improving change detection in forest areas based on stereo panchromatic imagery using kernel MNF,” *IEEE Transactions on Geoscience and Remote Sensing*, vol. 52, no. 11, pp. 7130–7139, 2014.
- [6] Corey Baker, Rick L Lawrence, Clifford Montagne, and Duncan Patten, “Change detection of wetland ecosystems using landsat imagery and change vector analysis,” *Wetlands*, vol. 27, no. 3, pp. 610–619, 2007.
- [7] Andreas Schmitt and Brian Brisco, “Wetland monitoring using the curvelet-based change detection method on polarimetric SAR imagery,” *Water*, vol. 5, no. 3, pp. 1036–1051, 2013.
- [8] Prosper Washaya, Timo Balz, and Bahaa Mohamadi, “Coherence change-detection with Sentinel-1 for natural and anthropogenic disaster monitoring in urban areas,” *Remote Sensing*, vol. 10, no. 7, pp. 1026, 2018.

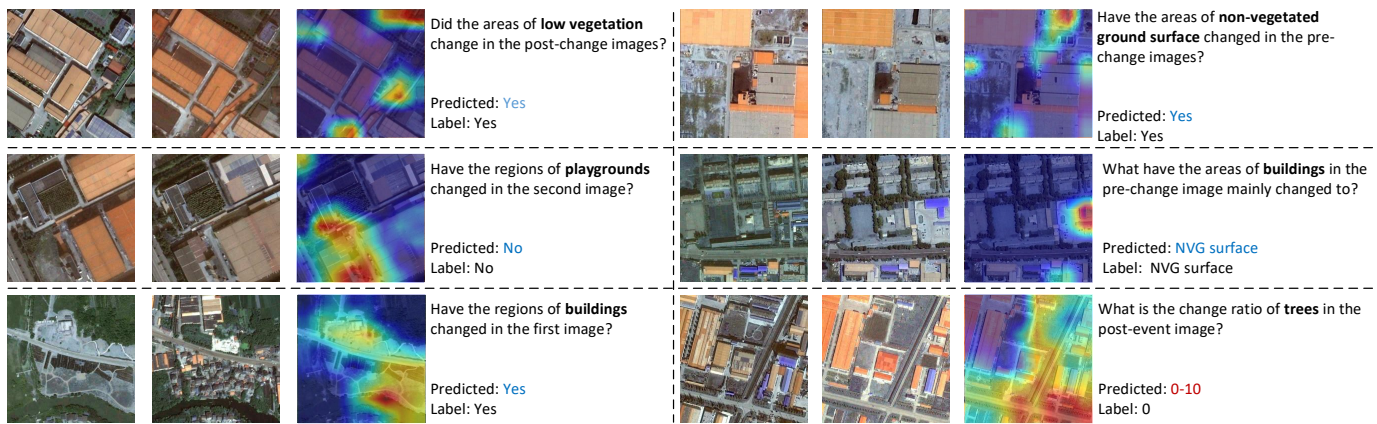


Fig. 10. Visualization examples of change attention maps. Best viewed in color.

- [9] Huijiao Qiao, Xue Wan, Youchuan Wan, Shengyang Li, and Wanfeng Zhang, "A novel change detection method for natural disaster detection and segmentation from video sequence," *Sensors*, vol. 20, no. 18, pp. 5076, 2020.
- [10] A-M Olteanu-Raimond, L See, M Schultz, G Foody, M Riffler, Tanja Gasber, Laurence Jolivet, Arnaud Le Bris, Yann Meneroux, Lanfa Liu, et al., "Use of automated change detection and VGI sources for identifying and validating urban land use change," *Remote Sensing*, vol. 12, no. 7, pp. 1186, 2020.
- [11] Bhogendra Mishra and Junichi Susaki, "Sensitivity analysis for l-band polarimetric descriptors and fusion for urban land cover change detection," *IEEE Journal of selected topics in applied earth observations and remote sensing*, vol. 7, no. 10, pp. 4231–4242, 2014.
- [12] Barry Haack, James Wolf, and Richard English, "Remote sensing change detection of irrigated agriculture in Afghanistan," *Geocarto international*, vol. 13, no. 2, pp. 65–75, 1998.
- [13] Sicong Liu, Daniele Marinelli, Lorenzo Bruzzone, and Francesca Bovolo, "A review of change detection in multitemporal hyperspectral images: Current techniques, applications, and challenges," *IEEE Geoscience and Remote Sensing Magazine*, vol. 7, no. 2, pp. 140–158, 2019.
- [14] Bo Du, Lixiang Ru, Chen Wu, and Liangpei Zhang, "Unsupervised deep slow feature analysis for change detection in multi-temporal remote sensing images," *IEEE Transactions on Geoscience and Remote Sensing*, vol. 57, no. 12, pp. 9976–9992, 2019.
- [15] Xuelong Li, Zhenghang Yuan, and Qi Wang, "Unsupervised deep noise modeling for hyperspectral image change detection," *Remote Sensing*, vol. 11, no. 3, pp. 258, 2019.
- [16] Zhiyong Lv, Tongfei Liu, and Jón Atli Benediktsson, "Object-oriented key point vector distance for binary land cover change detection using VHR remote sensing images," *IEEE Transactions on Geoscience and Remote Sensing*, vol. 58, no. 9, pp. 6524–6533, 2020.
- [17] Qi Wang, Zhenghang Yuan, Qian Du, and Xuelong Li, "GETNET: A general end-to-end 2-D CNN framework for hyperspectral image change detection," *IEEE Transactions on Geoscience and Remote Sensing*, vol. 57, no. 1, pp. 3–13, 2018.
- [18] Kunping Yang, Gui-Song Xia, Zicheng Liu, Bo Du, Wen Yang, Marcello Pelillo, and Liangpei Zhang, "Asymmetric siamese networks for semantic change detection in aerial images," *IEEE Transactions on Geoscience and Remote Sensing*, vol. 60, 2021.
- [19] Lei Ding, Haitao Guo, Sicong Liu, Lichao Mou, Jing Zhang, and Lorenzo Bruzzone, "Bi-temporal semantic reasoning for the semantic change detection in HR remote sensing images," *IEEE Transactions on Geoscience and Remote Sensing*, vol. 60, 2022.
- [20] Aditya Mogadala, Marimuthu Kalimuthu, and Dietrich Klakow, "Trends in integration of vision and language research: A survey of tasks, datasets, and methods," *arXiv preprint arXiv:1907.09358*, 2019.
- [21] Aditya Khamparia, Babita Pandey, Shrasti Tiwari, Deepak Gupta, Ashish Khanna, and Joel JPC Rodrigues, "An integrated hybrid CNN–RNN model for visual description and generation of captions," *Circuits, Systems, and Signal Processing*, vol. 39, no. 2, pp. 776–788, 2020.
- [22] Francis Ferraro, Nasrin Mostafazadeh, Ishan Misra, Aishwarya Agrawal, Jacob Devlin, Ross Girshick, Xiaodong He, Pushmeet Kohli, Dhruv Batra, C Lawrence Zitnick, et al., "Visual storytelling," *arXiv preprint arXiv:1604.03968*, 2016.
- [23] Stanislaw Antol, Aishwarya Agrawal, Jiasen Lu, Margaret Mitchell, Dhruv Batra, C Lawrence Zitnick, and Devi Parikh, "VQA: Visual question answering," in *IEEE International Conference on Computer Vision (ICCV)*, 2015, pp. 2425–2433.
- [24] Qi Wu, Damien Teney, Peng Wang, Chunhua Shen, Anthony Dick, and Anton van den Hengel, "Visual question answering: A survey of methods and datasets," *Computer Vision and Image Understanding*, vol. 163, pp. 21–40, 2017.
- [25] Tao Tu, Qing Ping, Govindarajan Thattai, Gokhan Tur, and Prem Natarajan, "Learning better visual dialog agents with pretrained visual-linguistic representation," in *IEEE/CVF Conference on Computer Vision and Pattern Recognition (CVPR)*, 2021, pp. 5622–5631.
- [26] Xiangtao Zheng, Binqiang Wang, Xingqian Du, and Xiaoqiang Lu, "Mutual attention inception network for remote sensing visual question answering," *IEEE Transactions on Geoscience and Remote Sensing*, 2021.
- [27] Zhenghang Yuan, Lichao Mou, and Xiao Xiang Zhu, "Self-paced curriculum learning for visual question answering on remote sensing data," in *2021 IEEE International Geoscience and Remote Sensing Symposium IGARSS*. IEEE, 2021, pp. 2999–3002.
- [28] Bo Qu, Xuelong Li, Dacheng Tao, and Xiaoqiang Lu, "Deep semantic understanding of high resolution remote sensing image," in *2016 International conference on computer, information and telecommunication systems (Cits)*. IEEE, 2016, pp. 1–5.
- [29] Xiaoqiang Lu, Binqiang Wang, Xiangtao Zheng, and Xuelong Li, "Exploring models and data for remote sensing image caption generation," *IEEE Transactions on Geoscience and Remote Sensing*, vol. 56, no. 4, pp. 2183–2195, 2017.
- [30] Chenyang Liu, Rui Zhao, and Zhenwei Shi, "Remote-sensing image captioning based on multilayer aggregated transformer," *IEEE Geoscience and Remote Sensing Letters*, vol. 19, 2022.
- [31] Sylvain Lobry, Diego Marcos, Jesse Murray, and Devis Tuia, "RSVQA: Visual question answering for remote sensing data," *IEEE Transactions on Geoscience and Remote Sensing*, vol. 58, no. 12, pp. 8555–8566, 2020.
- [32] Zhenghang Yuan, Lichao Mou, Qi Wang, and Xiao Xiang Zhu, "From easy to hard: Learning language-guided curriculum for visual question answering on remote sensing data," *IEEE Transactions on Geoscience and Remote Sensing*, vol. 60, 2022.
- [33] Kaifeng He, Xiangyu Zhang, Shaoqing Ren, and Jian Sun, "Deep residual learning for image recognition," in *IEEE/CVF Conference on Computer Vision and Pattern Recognition (CVPR)*, 2016, pp. 770–778.
- [34] Ashish Vaswani, Noam Shazeer, Niki Parmar, Jakob Uszkoreit, Llion Jones, Aidan N Gomez, Lukasz Kaiser, and Illia Polosukhin, "Attention is all you need," in *Advances in neural information processing systems (NeurIPS)*, 2017, pp. 5998–6008.
- [35] Igor V Tetko, Pavel Karpov, Ruud Van Deursen, and Guillaume Godin, "State-of-the-art augmented NLP transformer models for direct and single-step retrosynthesis," *Nature Communications*, vol. 11, no. 1, pp. 1–11, 2020.

- [36] Ze Liu, Yutong Lin, Yue Cao, Han Hu, Yixuan Wei, Zheng Zhang, Stephen Lin, and Baining Guo, “Swin transformer: Hierarchical vision transformer using shifted windows,” *arXiv preprint arXiv:2103.14030*, 2021.
- [37] Alexey Dosovitskiy, Lucas Beyer, Alexander Kolesnikov, Dirk Weissenborn, Xiaohua Zhai, Thomas Unterthiner, Mostafa Dehghani, Matthias Minderer, Georg Heigold, Sylvain Gelly, et al., “An image is worth 16x16 words: Transformers for image recognition at scale,” in *International Conference on Learning Representations (ICLR)*, 2021.
- [38] Nicolas Carion, Francisco Massa, Gabriel Synnaeve, Nicolas Usunier, Alexander Kirillov, and Sergey Zagoruyko, “End-to-end object detection with transformers,” in *European Conference on Computer Vision (ECCV)*, 2020, pp. 213–229.
- [39] Enze Xie, Wenhui Wang, Zhiding Yu, Anima Anandkumar, Jose M Alvarez, and Ping Luo, “Segformer: Simple and efficient design for semantic segmentation with transformers,” *arXiv preprint arXiv:2105.15203*, 2021.
- [40] Zhitong Xiong, Yuan Yuan, and Qi Wang, “MSN: Modality separation networks for RGB-D scene recognition,” *Neurocomputing*, vol. 373, pp. 81–89, 2020.
- [41] Yun Liu, Xiaoming Zhang, Qianyun Zhang, Chaozhuo Li, Feiran Huang, Xianghong Tang, and Zhoujun Li, “Dual self-attention with co-attention networks for visual question answering,” *Pattern Recognition*, vol. 117, pp. 107956, 2021.
- [42] Zhitong Xiong, Yuan Yuan, and Qi Wang, “ASK: Adaptively selecting key local features for RGB-D scene recognition,” *IEEE Transactions on Image Processing*, vol. 30, pp. 2722–2733, 2021.
- [43] Christel Chappuis, Sylvain Lobry, Benjamin Kellenberger, Bertrand Le Saux, and Devis Tuia, “How to find a good image-text embedding for remote sensing visual question answering?,” *arXiv preprint arXiv:2109.11848*, 2021.
- [44] Ryan Kiros, Yukun Zhu, Russ R Salakhutdinov, Richard Zemel, Raquel Urtasun, Antonio Torralba, and Sanja Fidler, “Skip-thought vectors,” *Advances in neural information processing systems*, vol. 28, 2015.
- [45] Ruizhe Shao, Chun Du, Hao Chen, and Jun Li, “SUNet: Change detection for heterogeneous remote sensing images from satellite and UAV using a dual-channel fully convolution network,” *Remote Sensing*, vol. 13, no. 18, pp. 3750, 2021.